Okamoto, Taka-aki; Nezu, Iehisa; Sanjou, Michio

PIV Measurement of Turbulence Structure and Monami Phenomena in Open-Channel Flows with Flexible Vegetations

PIV MEASUREMENTS OF TURBULENCE STRUCTURE AND MONAMI PHENOMENA IN OPEN-CHANNEL FLOWS WITH FLEXIBLE VEGETATIONS

Taka-aki Okamoto [1], Iehisa Nezu [2] and Michio Sanjou [3]

[1]Ph. D. student, Department of Civil Engineering, Kyoto University
Katsura Campus, Kyoto 615-8540, Japan, e-mail: takaakiokamoto@t02.mbox.media.kyoto-u.ac.jp
[2] Professor, Department of Civil Engineering, Kyoto University
Katsura Campus, Kyoto 615-8540, Japan, e-mail: Iehisa.Nezu@mbox.kudpc.kyoto-u.ac.jp
[3] Assistant Professor , Department of Civil Engineering, Kyoto University
Katsura Campus, Kyoto 615-8540, Japan, e-mail: sanjou@mbox.kudpc.kyoto-u.ac.jp

ABSTRACT

Turbulence structure in actual rivers is often affected by the presence of vegetation zone. These aquatic plants decrease flow velocity significantly within the canopy, and consequently a strong shear layer is formed between the over- and within-canopy layers. Coherent turbulent motions are also generated predominantly in the shear layer near the top of canopy. These organized vortices may have an essentially important relation with the waving motions of flexible vegetation, which is called here as the ''Monami''. Because these Monami motions govern the turbulent transport such as momentum, water quality and suspended sediment, it is necessary in echo hydraulics to investigate turbulence structure and Monami phenomena in open-channel flows with flexible vegetations.

Keywords: Turbulence structure, organized vortices, flexible vegetation, Monami phenomena

1. INTRODUCTION

Aquatic plants in actual rivers are the essentially important components of many ecosystems. In vegetated open-channel flow, the time-averaged velocity profile contains the inflection point, and consequently, the Kelvin-Helmholtz instability generates the large-scale organized vortices, which dominates the transfer of momentum and scalar concentration through the canopy layer, e.g. see a review of Finnigan(2000). It is considered then that the downstream convection of coherent vortices causes the coherent waving motions of aquatic vegetation, that is called here the 'Monami'.

Hydrodynamic characteristics in open-channel flows with flexible vegetation have recently been investigated. For example, Ackerman & Okubo (1993) investigated the effect of a marine plant canopy on flow structure by using a dual-sensor electromagnetic current meter. They revealed that the periodic velocity fluctuations were caused by the plant movement and that mixing rate was reduced within the canopy. Brunet et al.(1993) have measured the distributions of various single-point statistical moments in a wind tunnel with waving wheat models by hot-wire anemometers. They showed that the pressure diffusion term in the turbulence kinetic energy (TKE) acted significantly against turbulent diffusion just above and within the canopy.

Ghisalberti & Nepf (2002) have conducted turbulence measurements in open-channel flow with seagrass vegetation models on the basis of both of laser Doppler anemometer

Table.1 Hydraulic condition

case	H (cm)	h (cm)	U_m (cm/s)	Re	Fr	a (1/m)	classification of plant motion
DH7U20	7.0	7.0	20.0	14000	0.24	3.8	**Swaying(S)**
DH8.75U20	8.75			17500	0.22		
DH10.5U20	10.5			21000	0.20		**Monami(M)**
DH14U20	14.0			28000	0.17		
DH17.5U20	17.5			35000	0.15		
DH21U20	21.0			42000	0.14		
DH24.5U20	24.5			49000	0.13		
DH28U20	28.0			56000	0.12		
CH7U20	7.0			14000	0.24	7.6	**Swaying(S)**
CH8.75U20	8.75			17500	0.22		
CH10.5U20	10.5			21000	0.20		**Monami(M)**
CH14U20	14.0			28000	0.17		
CH17.5U20	17.5			35000	0.15		
CH21U20	21.0			42000	0.14		
CH24.5U20	24.5			49000	0.13		
CH28U20	28.0			56000	0.12		
CH14U8	14.0		8.0	11200	0.07		**Swaying(S)**
CH14U13			13.0	18200	0.11		

(LDA) and acoustic Doppler velocimetry (ADV). They found that the submerged vegetation flow resembles a mixing layer rather than a boundary layer. Further, Ghisalberti & Nepf (2006) conducted laboratory experiments with rigid and flexible vegetation model. They revealed that the coherent vortex consists of a strong sweep on its front side, followed by a week ejection on its backside by using a phase average analysis of the waving motion of vegetation elements. Recently, Nezu et al.(2007) conducted PIV measurements in vegetated open-channel flows with *rigid* vegetation models. They found that coherent eddies are more significantly organized at the vegetation edge than the within-canopy layer and the convection velocity is larger than the time-averaged mean flow velocity.

However, the important relation between Monami phenomena and the instantaneous turbulence structure is not yet available, since many researchers have studied vegetated flows on the basis of single-point statistics. In this study, we investigated the instantaneous turbulence structure and coherent motions in open-channel flows with flexible vegetation by using PIV&PTV techniques.

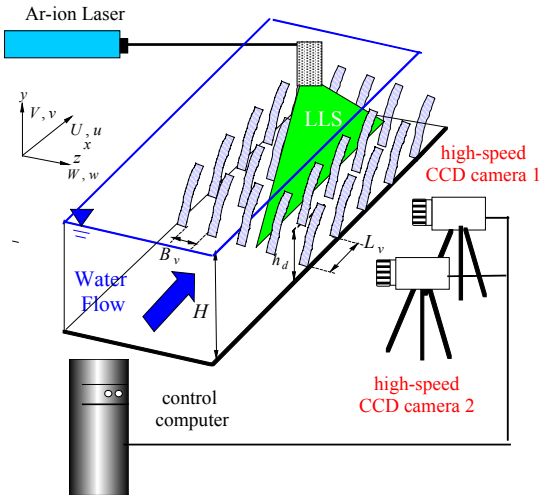

Fig.1 Experimental set-up

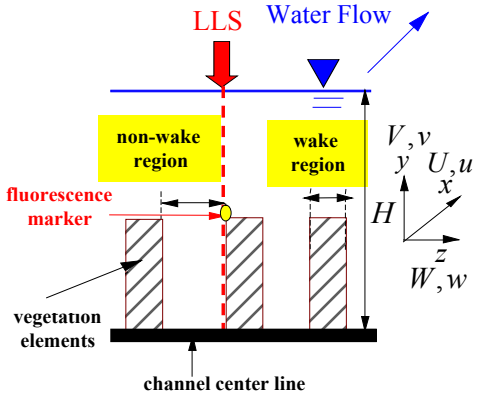

Fig.2 Travers line of illuminated plane by LLS

2. EXPERIMENTAL METHOD

Fig.1 shows the experimental setup and the coordinate system. The present experiments were conducted in a 10m long and 40cm wide tilting flume. Flexible vegetation elements were made of 70mm height, 8mm wide and 0.1mm thick OHP film strip sheets.

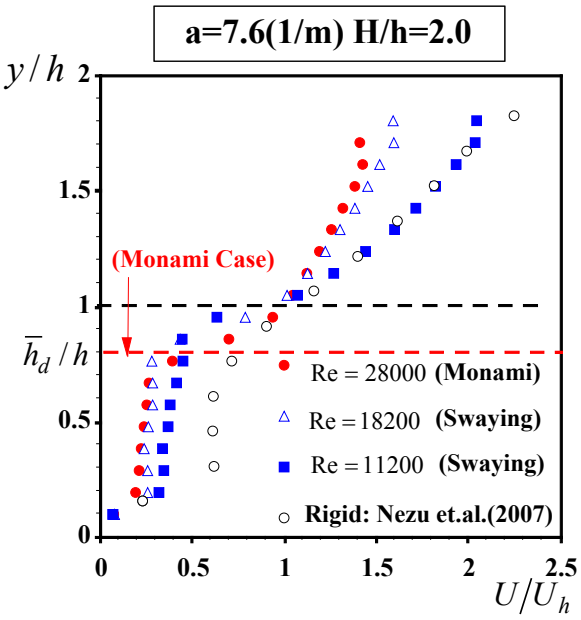

Fig. 3 Streamwise velocity profile

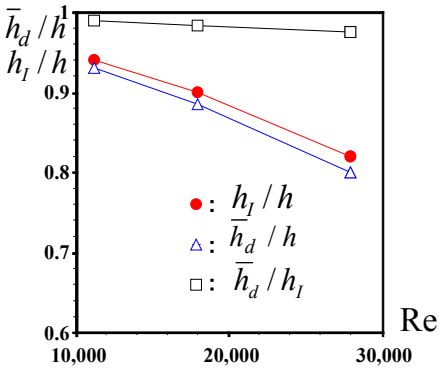

Fig. 4 Deflected height $\overline{h}_d$

H is the water depth, h is the vegetation height and $\overline{h}_d$ is the time-averaged deflected height of flexible vegetation element. L_v and B_v are the neighboring vegetation spacings in the streamwise and spanwise directions, respectively. x, y and z are the streamwise, vertical and spanwise coordinates, respectively. The vertical origin, $y = 0$, is chosen as the channel bed. The time-averaged velocity components in each direction are defined as U, V and W, and the turbulent fluctuations are u, v and w, respectively.

In the present study, two components of instantaneous fluid velocity $(\tilde{u}, \tilde{v})$ and the flexible vegetation motions of flexible strip elements were measured simultaneously by two sets of high-speed cameras. A laser light sheet (LLS) was projected into the water column vertically from the free surface at 7m downstream from the channel entrance (Fig.1). The 2mm thick LLS was generated by 3W argon-ion laser using a cylindrical lens. The illuminated flow images were taken by CMOS camera (1000×1000pixels) with 500Hz frame-rate and 60s sampling time. The instantaneous velocity vectors on the x-y plane were calculated by the PIV algorithm for the whole depth region, in the same way as used by Nezu et.al. (2007). Two CMOS cameras were arranged in order to cover a wide measuring area (the total streamwise length was 600mm and the overlapped zone was 60mm). The instantaneous motion of the flexible vegetation elements was analysed by PTV technique. The fluorescence marker was attached on the corner edge of the vegetation element as shown in Fig.2, and the laser light sheet was projected on the markers from the free surface. Consequently, the tip motion of vegetations was easily analysed by the PTV. The instantaneous measurements of water velocity and vegetation motion were successfully conducted by the PIV & PTV techniques.

Table 1 shows the hydraulic condition. Experiments were conducted on the basis of several flow scenarios, in which the relative submergence depth H/h, the bulk mean velocity U_m and the vegetation density a were changed. The classification of plant motions is indicated in Table 1. 'S' means *Gently Swaying*, and 'M' means *Monami (organized waving)*.

In this study, the vegetation density a is defined as follows:

$$a = \frac{total \quad frontal \quad area}{volume \quad of \quad vegetation \quad zone} = \frac{\sum_i A_i}{S \cdot h} \tag{1}$$

in which, A_i is the frontal area of the vegetation models and S is the referred bed area.

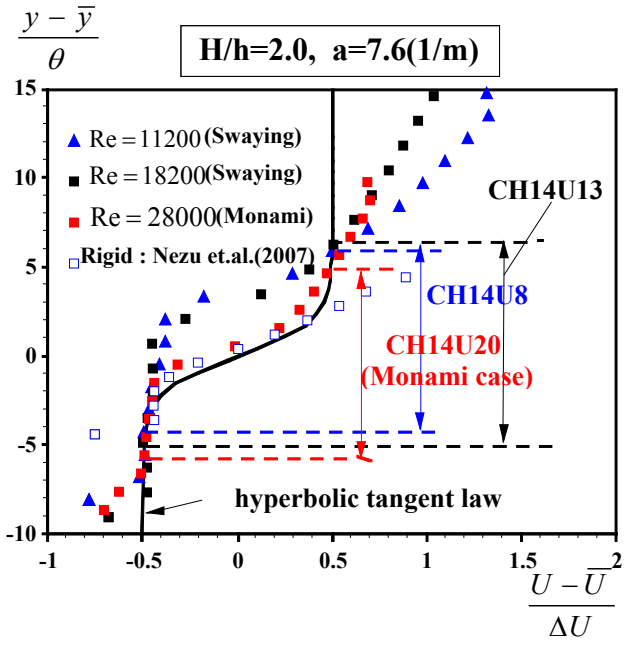

Fig. 5 Comparison of the present mean velocity values with tangent hyperbolic law of mixing layer

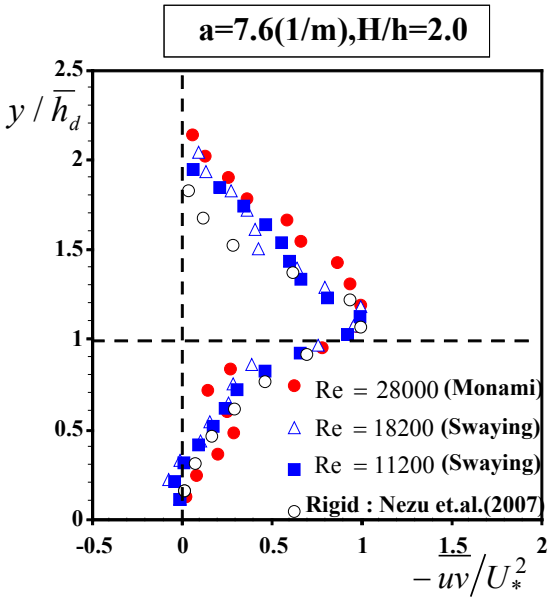

Fig. 6 Reynolds stress distribution

3. RESULTS

3.1 Mean Velocity Profile and Reynolds Stress Distribution

Fig.3 shows the vertical profiles of the streamwise velocity component $U(y)$ for the rigid vegetation flow measured by Nezu et al. (2007) and the present flexible ones. The results are normalized by the tip velocity at the vegetation edge, U_h. The velocity profiles show almost constant velocity values within the canopy near the channel bed and an inflection point appears near the vegetation tip (y=h for rigid canopy and y=$\overline{h}_d$ for flexible one). The time-averaged deflected height $\overline{h}_d$ and the height of the inflection point h_I are shown in Fig.4. It is found that both of $\overline{h}_d$ and h_I decrease with an increase of Reynolds number Re.

Fig.5 compares the mean velocity profiles of the rigid and flexible vegetation flows with the hyperbolic tangent law of mixing layers. The velocity profile of pure mixing layers is give by.

$$\frac{U-\overline{U}}{\Delta U}=\frac{1}{2}\tanh\left(\frac{y-\overline{y}}{2\theta}\right) \qquad (2)$$

in which, $\overline{U}=1/2\left(U_1+U_2\right)$, $\Delta U=(U_2-U_1)$ and θ is the momentum thickness. U_1 is the constant velocity of the low speed zone in mixing layer and U_2 is the constant one of the high speed zone. It is found that the results of the Monami cases (Re=28000) and the rigid canopy case resemble the mixing-layer profile more closely than the Swaying case (Re=11200, and 18000). The analogy between the canopy shear layer and the mixing shear layer becomes more significant when the Monami phenomena are observed.

Fig.6 shows the vertical distribution of the Reynolds shear stress $-\overline{uv}$ normalized by the deflected height $\overline{h}_d$ for rigid canopy, Swaying (Re=11200, and 18000) and Monami case (Re=28000). U_* was defined as the peak value of $-\overline{uv}$, as conducted by Nezu et al.

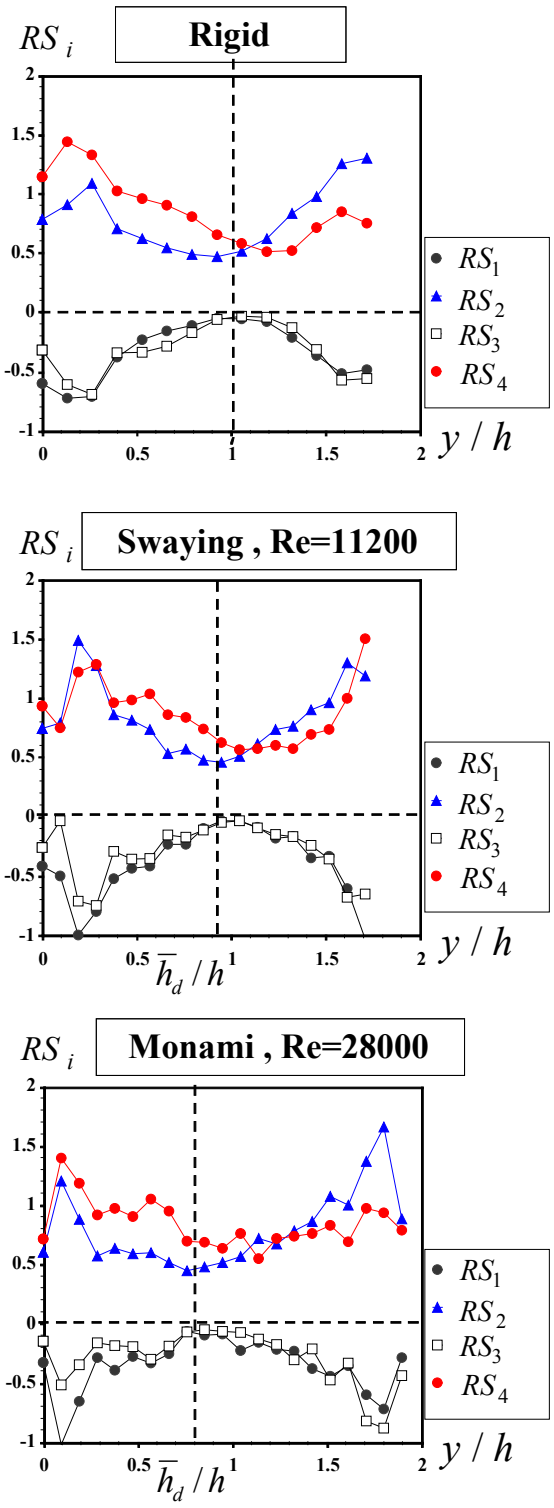

Fig. 7 Conditional Reynolds stress contribution

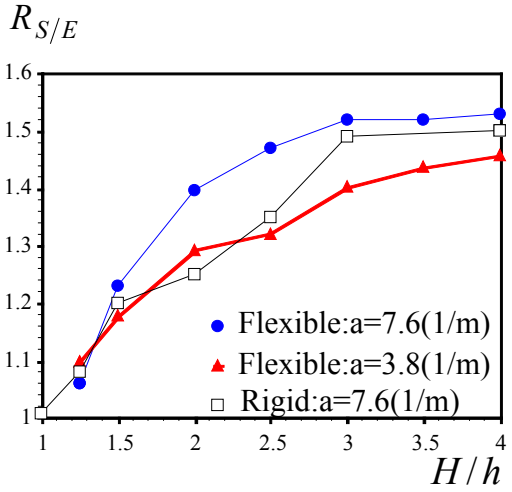

Fig. 8 $R_{S/E}$ against the submergence depth

(2007). It was found clearly that the distribution for the Swaying case is similar to the rigid canopy one with a sharp peak near the vegetation edge. In contrast, the Monami case has a milder peak structure, which is consistent with Ghisalberti & Nepf (2006)'s data.

3.2 Conditional analysis

The quadrant conditional analysis was conducted to evaluate the impact of vegetation flexibility on the turbulence structure. All event contributions to the Reynolds stress are classified, as follows:

i=1 $(u>0, v>0)$: outward interaction
i=2 $(u<0, v>0)$: ejection
i=3 $(u>0, v<0)$: inward interaction
i=4 $(u<0, v<0)$: sweep

The normalized contribution to the Reynolds stress from the *i*-th quadrant event is given by:

$$RS_i = \left(\overline{uv}\right)^{-1} \lim_{T\to\infty} \frac{1}{T} \int_0^T uvI_i\, dt \qquad (3)$$

,which I_i is the detection function, e.g. see Nezu & Nakagawa (1993).

Fig.7 shows the values of RS_i for the rigid canopy, Swaying (*Re*=11200) and Monami cases (*Re*=28000). It is evident from Fig.7 that RS_4 is larger than RS_2 within the

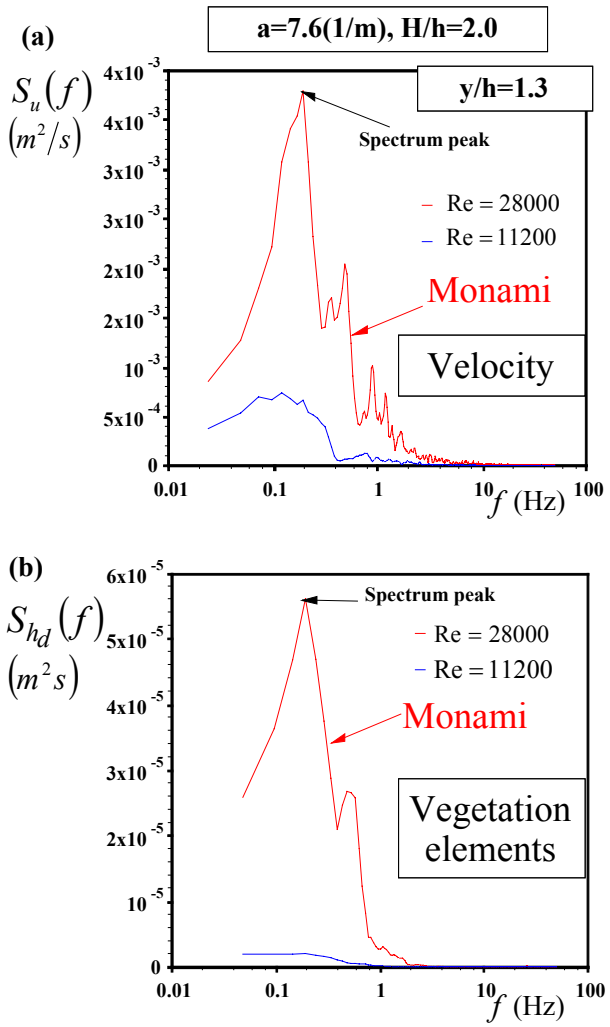

Fig. 9 (a) Spectrum of the streamwise velocity component
(b) Spectrum of the deflected height of vegetation

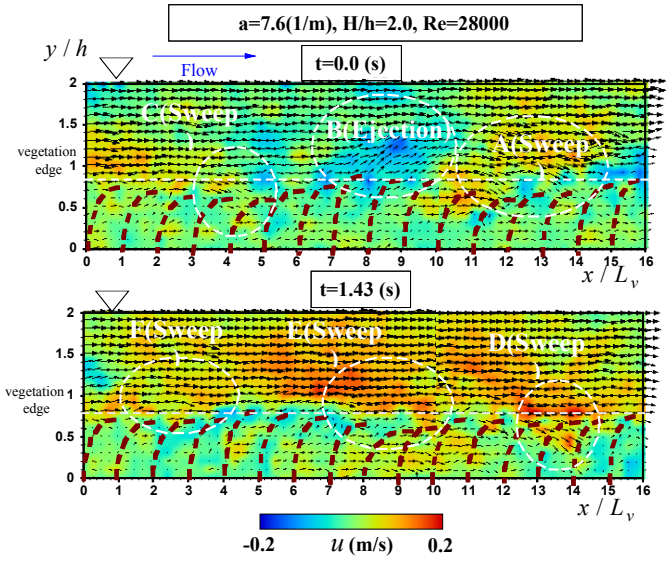

Fig. 10 Instantaneous velocity vectors

flexible canopy. This suggests that the structure of the quadrant contributions for flexible vegetation is similar to that for rigid one. The sweep events are more dominant in the Monami case than in the Swaying case. When the Monami appears, the vertical transport of the high-speed fluid parcel toward the canopy layer is promoted more significantly.

In order to evaluate the contributions of sweeps and ejections, Ghisalberti & Nepf (2006) proposed the following parameter $R_{S/E}$.

$$R_{S/E} = \frac{1}{h - h_p}\int_{h_p}^{h} (RS_4 / RS_2)dz \qquad (4)$$

Fig.8 shows the variation of $R_{S/E}$ against the vegetation submergence depth H/h. It is found that the contribution of sweeps becomes more significant than the ejections as the submergence depth H/h increases. This indicates that as the depth ratio increases, a shear layer develops at the top of the canopy and sweeps dominate ejections within the canopy.

3.3 Spectral Analysis

Fig.9 (a) shows the power spectrum of the streamwise velocity $u(t)$ at y/h=1.3 (above canopy region) for the Swaying and Monami case (H/h=2.0). This figure shows that one spectral peak appears significantly in the low frequency band between 0.1 and 0.2Hz in the Monami case (Re=28000). In contrast, any typical spectral peak cannot be observed in the Swaying case (Re=11200). This predominant peak corresponds well

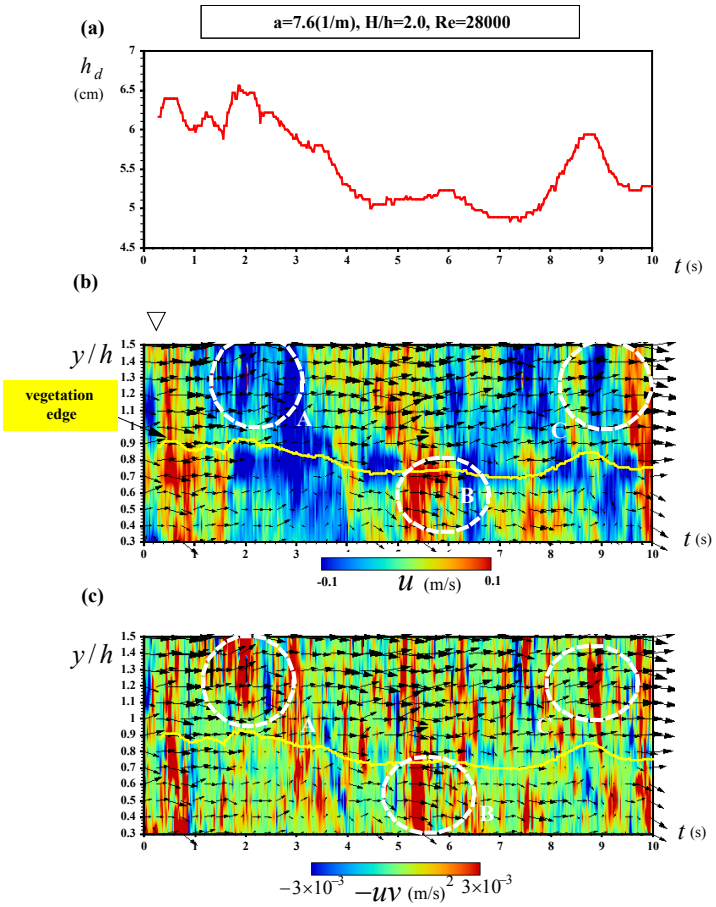

Fig. 11 Time series of the deflected height (a), instantaneous velocity vectors (b), instantaneous Reynolds stress (c)

to the predicted K-H frequency f_{KH}, which is given by.

$$f_{Kh} = \frac{0.032\overline{U}}{\theta} \tag{5}$$

Such a good agreement of (5) with measurements is also pointed out by Ikeda & Kanazawa (1996). Fig.9 (b) shows the power spectrum of the fluctuations of deflected element height $h_d(t)$ for the Swaying and Monami case (H/h=2.0), which could be evaluated by PTV. The Monami frequency is in good agreement with the peak frequency in velocity spectrum in the Monami. The agreement of these frequencies between velocity and vegetation fluctuations confirms that the waving motion of vegetation is associated with the strong oscillation in streamwise velocity. Consequently, it is suggested that coherent eddies generate the Monami motion pf vegetation, which could be evaluated by PTV.

3.4 Correlation between the Flow Structure and the Vegetation Motion

Fig.10 shows an example of the instantaneous velocity vectors $(\tilde{u}, \tilde{v})$ for the Monami case (H/h=2.0. The colored contour indicates the value of the instantaneous velocity fluctuations $u(x, y, t)$. The sweep motion, i.e., the downward high-speed fluid ($u > 0$ and $v < 0$), is observed (dashed circle 'A', 'C', 'D', 'E' and 'F'), and it is followed by the ejection motion (dashed circle 'B'), i.e., the upward vectors of low-speed fluid. It is recognized that there is a periodical pattern of the sweep and ejection motions in the Monami case.

Fig.11 (a) shows the time series of the deflected vegetation height $h_d(t)$ in the Monami (H/h=2.0). Fig.11 (b) and (c) show the time series of the instantaneous velocity vectors $(\tilde{u}, \tilde{v})$ and the instantaneous Reynolds stress $-uv$, respectively. The yellow line indicates the height of instantaneous canopy top h_d. At $t = 2.0$ s, the ejection motion appears above the instantaneous canopy tip, which is indicated by a dashed circle "A". It is found in Fig.11 (c) that a large distribution of $-uv$ is observed locally in the dashed circle "A". At $t = 6.0$ s, h_d decreases and the vegetation is deflected most significantly. Then, the sweep motion (dashed circle "B") appears below the vegetation tip. At $t = 9.0$ s, h_d increases and ejection lump appears again (dashed circle "C") above the vegetation edge. These results suggest that large positive regions of the instantaneous Reynolds stress are consistent well

with these lump structures of coherent motions and the greatest vertical transport of large-scale coherent turbulence occurs when the vegetation height attains at its minimum and maximum.

4. CONCLUSIONS

In the present study, two components of instantaneous fluid velocity and the flexible vegetation motions were measured simultaneously by using both of PIV and PTV in open-channel flows with flexible vegetation. As the results, mean-flow properties, turbulence structure and coherent motions were revealed and discussed. Main findings obtained in the present study obtained in the present study are as follows:

1) For flexible vegetation, the time-averaged deflected height and the inflection-point height decrease with increase of Reynolds number. The Reynolds stress distribution has a milder peak structure in the Monami case.
2) It was found that the analogy between the canopy shear layer and the mixing shear layer becomes more significant when the Monami phenomena are observed
3) Conditional analysis revealed that the vertical transport for both rigid and flexible vegetations is more dominated by sweep motions than the ejection ones.
4) Spectral analysis revealed that the Monami frequency of vegetation is in good agreement with the peak frequency of velocity for the Monami.
5) There is a periodical property of the sweep and ejection motions near the vegetation tip in the Monami case. The greatest vertical transport of large-scale turbulence occurs when the canopy vegetation elements are deformed at its minimum and maximum.

REFERENCES

1) Ackerman, J., Okubo, A. (1993): Reduced mixing in a marine macrophyte canopy, *Funct. Ecol*., Vol. 7, pp.305-309.
2) Brunet, Y., Finnigan, J.J. and Raupach, M.R. (1994): A wind tunnel study of air flow in waving wheat: single-point velocity statistics, *Boundary Layer Meteorology,* Vol.70, pp.95-132.
3) Finnigan J.(2000): Turbulence in Plant Canopies, *Ann. Rev. Fluid Mech.*, Vol. 32, pp.519-572.
4) Ghisalberti, M. and Nepf, H. (2002): Mixing layers and coherent structures in vegetated aquatic flows, *J. of Geophysical Res.,* Vol. 107, pp.3-1-3-11-
5) Ghisalberti, M. and Nepf, H. (2006) : The structure of the shear layer in flows over rigid and flexible canopies, *Environmental Fluid Mechanics,* Vol.6, pp.277-301.
6) Ho, C.M. and Huerre, P. (1984): Perturbed free shear layers, ANN. Rev. Fluid Mech., Vol.16, pp.365-424.
7) Ikeda, S. and Kanazawa, M. (1996) : Three-dimensional organized vortices above flexible water plants, *J. of Hydraulic Eng.,* Vol. 122(11), pp.634-640.
8) Nezu, I. and Nakagawa, H. (1993) : Turbulence in Open-Channel Flows, IAHR-Monograph, Balkema
9) Nezu, I., Sanjou, M. and Okamoto, T. (2007): PIV measurements in vegetated open-channel flows, proc.of 32nd, IAHR, Congress of Venice. No.466 (10pages on CD-ROM).